Quantum memory of single-photon polarization qubits via double electromagnetically induced transparency

Qi Zhang[1] and Guoxiang Huang[1,2,3]

[1]*State Key Laboratory of Precision Spectroscopy, East China Normal University, Shanghai 200062, China*
[2]*Collaborative Innovation Center of Extreme Optics, Shanxi University, Taiyuan 030006, China*
[3]*NYU-ECNU Joint Institute of Physics at NYU-Shanghai, Shanghai 200062, China*

(Received 13 April 2021; revised 5 September 2021; accepted 13 September 2021; published 24 September 2021)

We present a theoretical investigation on the quantum memory of photonic polarization qubits via electromagnetically induced transparency (EIT). The system we consider is a tripod-shaped four-level atomic system working under the condition of a double EIT, by which the storage and retrieval of a single-photon polarization qubit are implemented through the switching off and on of a control laser field, and the storage efficiency and the quantum-state fidelity for qubit memory are both calculated. We show that the optimal optical depth for acquiring the maximum efficiency and maximum fidelity of the qubit memory can be obtained simultaneously, which can be further improved by suppressing the optical absorption and dispersion via the choice of the time duration of the input qubit pulse and the amplitude of the control field. We also carry out a calculation on the quantum memory of a single-photon qudit by considering a multipod-shaped atomic-level configuration. The results reported here are useful for understanding the quantum transmission property of slow lights with multiple components and helpful for experimental realizations of high-quality memory of photonic qubits and qudits.

DOI: 10.1103/PhysRevA.104.033714

I. INTRODUCTION

Quantum memories (QMs), devices that can efficiently store and retrieve the quantum states on demand, play crucial roles in quantum information processing, especially in the implementation of repeater-based long-distance quantum communications, the enhancement of the precision of quantum metrology, the conversion of the heralded quantum states into on-demand quantum states, and the synchronization of the operations in quantum computations [1–7]. One of the important QM techniques is electromagnetically induced transparency (EIT), occurring typically in three-level atomic gases in which typical quantum interference effect induced by a strong control laser field leads to the propagation of a weak signal laser field with significant suppression of optical absorption and slowdown of group velocity [8]. Based on the theory of dark-state polaritons, the storage and retrieval of the signal field can be realized by switching off and on the control field in an adiabatical and successive way [9]. Since the first experimental realization [10,11], much effort has been paid to the storage and retrieval of optical pulses using EIT [12–23].

It is well known that EIT enables the preservation of quantum properties of light [24,25], which can be utilized for the storage and retrieval of nonclassical light [26–34]. In particular, the QMs of photonic qubits are able to encode quantum information with the superposition of two-dimensional degrees of freedom of a photon (such as polarizations, orbital angular momentum, path, time bins, etc.) [35]. Among them, polarization degrees of freedom are particularly convenient for codings and have been demonstrated to allow reliable and robust transmission and QMs of single-photon qubits [36–51].

The storage efficiency and the quantum-state fidelity are two key physical parameters for characterizing the quality of QMs, and a high-quality QM should have storage efficiency and quantum-state fidelity both close to unity in principle. In recent years, a number of theoretical investigations on QM efficiency have been proposed [52–57]. Nevertheless, a systematical theoretical study on both of these two parameters and their optimizations in processes of QMs is still lacking. Although quantum-state fidelities are commonly measured experimentally by exploiting the technique of quantum tomography [58,59], the results acquired by such a technique give no information on dynamical processes of QMs.

In this paper, we investigate the photon QMs by considering the storage and retrieval of single-photon polarization qubits in a cold, tripod-shaped four-level atomic gas working under the condition of double EIT. The storage efficiency η and the quantum-state fidelity F of the qubit memory are both calculated and optimized. We show that an optimal optical depth for achieving the maximum efficiency $\eta_{\max}$ and the maximum quantum-state fidelity $F_{\max}$ for the qubit memory can be obtained simultaneously; moreover, $\eta_{\max}$ and $F_{\max}$ can be improved by suppressing the optical absorption and dispersion via the choice of the time duration of the input qubit pulse and the amplitude of the control field, both of which can reach nearly 0.88 for ^{87}Rb atomic gas. We also carry out a theoretical calculation on the quantum memory of a single-photon qudit by considering a multipod-shaped atomic-level configuration, which is composed of three or more degrees of freedom of photons and is useful for increasing information-carrying capacity. A theoretical estimation of the optimized storage efficiency and quantum-state fidelity of the QM of single-photon qudits is provided.

Before proceeding, we would like to stress that our work is different from previously reported QMs using EIT [36–57]. (i) The theoretical investigation presented here is an all-quantum theoretical study of EIT-based qubit and qudit memories. (ii) The two polarization components of the photon qubit considered here are assumed to be stored and retrieved in a single atomic ensemble, which is different from the previous studies, where two remote atomic ensembles were employed [36,38,50]. (iii) At variance with the previous theoretical studies, the storage efficiency and the quantum-state fidelity are both calculated, and the optimal optical depth for obtaining the maximum efficiency and maximum fidelity of the qubit memory can be obtained simultaneously. (iv) The result for further improving the efficiency and fidelity of the qubit memory by adjusting the time duration of the input qubit wave packet and the control-field amplitude agrees with the experimental observation reported recently in Ref. [51].

The remainder of this paper is arranged as follows. In Sec. II, we describe the tripod-shaped atomic model under study and consider the linear propagation of single-photon qubit pulses. In Sec. III, we present analytical and numerical results on the efficiency and fidelity of the qubit memory and their optimizations. In Sec. IV, we extend the system to a multipod-shaped model and discuss the quantum memory of a single-photon qudit. Finally, in Sec. V we give a summary on the main results obtained in this paper.

II. MODEL AND PROPAGATION OF SINGLE-PHOTON POLARIZATION QUBITS

A. Physical model

We start by considering a cold atomic gas with a tripod-shaped four-level configuration interacting with a weak, pulsed signal laser field (central angular frequency ω_p) and a strong, control laser field (central angular frequency ω_c), both of which are assumed to propagate along the z direction so as to suppress the first-order Doppler effect; see Fig. 1(a). Level $|4\rangle$ is an excited state with spontaneous-emission decay rate Γ_4; $|1\rangle$, $|2\rangle$, and $|3\rangle$ are Zeeman-split sublevels of the atomic ground state, which are induced by a weak static external magnetic field $\mathbf{B}$ applied along the z direction [i.e., $\mathbf{B} = (0, 0, B_0)$]. The signal field is linearly polarized in the x-y plane, which can be taken as a linear superposition of the right-circularly (σ^+) and the left-circularly (σ^-) polarized components that couples the transitions $|1\rangle \leftrightarrow |4\rangle$ and $|2\rangle \leftrightarrow |4\rangle$, respectively. The control field is chosen to be linearly polarized, coupling to the transition $|3\rangle \leftrightarrow |4\rangle$. The level spacing between $|1\rangle$ and $|2\rangle$ is given by Δ_2 (an example will be given below); Δ_4 and Δ_3 are one- and two-photon detunings, respectively [60]. Note that in this tripod-shaped scheme there are two Λ-shaped excitation paths, i.e., $|1\rangle \rightarrow |4\rangle \rightarrow |3\rangle$ and $|2\rangle \rightarrow |4\rangle \rightarrow |3\rangle$, which constitute two standard Λ-shaped EITs (with state $|4\rangle$ being a shared excited state). Thus the dynamics of the signal field and the atoms in the system is essentially governed by a double EIT.

For simplicity, we assume that the signal field has a wide transverse spatial distribution [or the atomic gas is filled in a quasi-one-dimensional (quasi-1D) waveguide] so that the diffraction effect of the signal field can be neglected. Therefore a (1+1)D scheme (i.e., time plus space along the z direction) is sufficient to describe the dynamics of signal photons, as schematically shown in Fig. 1(b). The total electric field in the system reads

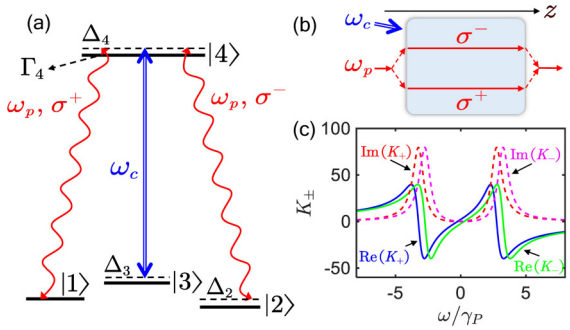

FIG. 1. (a) Energy-level diagram and excitation scheme of the tripod-shaped four-level atomic gas, proposed to realize the QM of a single-photon polarization qubit. The signal field with central angular frequency ω_p is decomposed into a superposition of right-circularly (σ^+) and left-circularly (σ^-) polarized components. ω_c is the central angular frequency of the control field used to realize the double EIT. Δ_4 and Δ_3 are one-photon and two-photon detunings, respectively. Γ_4 is the decay rate of spontaneous emission from the excited state $|4\rangle$. (b) Possible experimental geometry; both the signal and control fields propagate along the z direction. (c) Linear dispersion relation K_+ (K_-) of the σ^+ (σ^-)-polarized component of the signal field as a function of the sideband frequency ω; Re(K_j) and Im(K_j) are the real and imaginary parts of K_j ($j = +, -$), respectively. $\gamma_P = \gamma_{41} \approx \gamma_{42}$, where γ_{4j} ($j = 1, 2$) are the dephasing rates between the ground-state sublevel $|j\rangle$ and the excited state $|4\rangle$.

$$\hat{\mathbf{E}}(z,t) = \mathbf{E}_c(z,t) + \hat{\mathbf{E}}_p(z,t), \tag{1a}$$

$$\mathbf{E}_c(z,t) = \mathbf{e}_c \mathcal{E}_c(z,t) e^{i(k_c z - \omega_c t)} + \text{c.c.}, \tag{1b}$$

$$\hat{\mathbf{E}}_p(z,t) = \hat{\mathbf{E}}_{p+}(z,t) + \hat{\mathbf{E}}_{p-}(z,t), \tag{1c}$$

$$\hat{\mathbf{E}}_{pj}(z,t) = \mathbf{e}_{pj} \mathcal{E}_p \hat{E}_{pj}(z,t) e^{i(k_p z - \omega_p t)} + \text{H.c.}, \tag{1d}$$

with $j = +, -$. Here, $\mathbf{e}_c$ and $\mathcal{E}_c(z,t)$ are the unit polarization vector and the slowly varying envelope of the control field, respectively; $\mathcal{E}_p \equiv \sqrt{\hbar\omega_p/(2\varepsilon_0 V)}$ is the electric-field amplitude of a single signal photon, with $\mathbf{e}_{p+} = (\mathbf{e}_x + i\mathbf{e}_y)/\sqrt{2}$ [$\mathbf{e}_{p-} = (\mathbf{e}_x - i\mathbf{e}_y)/\sqrt{2}$] being the unit polarization vector of its σ^+ (σ^-)-polarized component; $\hat{E}_{p+}(z,t)$ [$\hat{E}_{p-}(z,t)$] is the longitudinal slowly varying annihilation operator of photons in the σ^+ (σ^-)-polarized component of the signal field, obeying the equal-time commutation relation $[\hat{E}_{pj}(z,t), \hat{E}^\dagger_{pj'}(z',t)] = L\delta(z-z')\delta_{jj'}$, with L being the quantization length along the z axis; and c.c. in expression (1b) [H.c. in (1d)] means complex (Hermitian) conjugate.

Under electric-dipole, rotating-waving, and paraxial approximations, the Hamiltonian of the system reads

$$\begin{aligned}\hat{H}^{\text{H}} = &-\frac{\hbar c}{L}\int_{-\infty}^{+\infty} dz\left[\hat{E}^\dagger_{p+}\left(i\frac{\partial}{\partial z}\right)\hat{E}_{p+} + \hat{E}^\dagger_{p-}\left(i\frac{\partial}{\partial z}\right)\hat{E}_{p-}\right] \\ &-\frac{\hbar N}{L}\int_{-\infty}^{+\infty} dz\left(\sum_{\alpha=1}^{4}\Delta_\alpha \hat{S}_{\alpha\alpha} + g_{p+}\hat{S}^\dagger_{14}\hat{E}_{p+}\right. \\ &\left. + g_{p-}\hat{S}^\dagger_{24}\hat{E}_{p-} + \Omega_c \hat{S}^\dagger_{34} + \text{H.c.}\right).\end{aligned} \tag{2}$$

Here, N is the atomic number in the system; $\hat{S}_{\alpha\beta}(z,t) = (\Delta N)^{-1}\sum_{j\in\Delta L}\hat{S}^j_{\alpha\beta}(t)$ $(\alpha = 1,2,3,4)$ are slowly varying collective atomic transition operators, with $\Delta N\,(\gg 1)$ being the atomic number within a small length ΔL; $\hat{S}^j_{\beta\alpha}(t) = \hat{\sigma}^j_{\beta\alpha}(t)\exp[i(k_\beta - k_\alpha)z_j - i(\omega_\beta + \Delta_\beta - \omega_\alpha - \Delta_\alpha)t]$ is the slowly varying atomic operator related to the transition $|\alpha\rangle \leftrightarrow |\beta\rangle$ of the jth atom [61], obeying the equal-time commutation relation

$$[\hat{S}_{\alpha\beta}(z,t), \hat{S}_{\alpha'\beta'}(z',t)] = \frac{L}{N}\delta(z-z')[\delta_{\alpha'\beta}\hat{S}_{\alpha\beta'}(z,t) - \delta_{\alpha\beta'}\hat{S}_{\alpha'\beta}(z,t)]; \tag{3}$$

$g_{p+} = (\mathbf{e}_{p+}\cdot\mathbf{p}_{41})\mathcal{E}_p/\hbar$ $[g_{p-} = (\mathbf{e}_{p-}\cdot\mathbf{p}_{42})\mathcal{E}_p/\hbar]$ is the coefficient denoting the dipole coupling between the σ^+ (σ^-)-polarized component of the signal photon and the atomic transition $|1\rangle \leftrightarrow |4\rangle$ $(|2\rangle \leftrightarrow |4\rangle)$, i.e., single-photon half Rabi frequency; $\Omega_c \equiv (\mathbf{e}_c\cdot\mathbf{p}_{43})\mathcal{E}_c/\hbar$ is the half Rabi frequency of the control field, with $\mathbf{p}_{\alpha\beta}$ being the electric-dipole matrix element associated with the transition $|\alpha\rangle \leftrightarrow |\beta\rangle$; and the detunings are defined by $\Delta_2 = \omega_1 - \omega_2$, $\Delta_3 = \omega_p - \omega_c - (\omega_3 - \omega_1)$, $\Delta_4 = \omega_p - (\omega_4 - \omega_1)$, with $\hbar\omega_\alpha$ being the eigenenergy of the atomic state $|\alpha\rangle$.

The dynamics of the system is governed by the Heisenberg-Langevin and Maxwell (HLM) equations, reading

$$i\frac{\partial}{\partial t}\hat{S}_{\alpha\beta} = \left[\hat{S}_{\alpha\beta}, \frac{\hat{H}^{\mathrm{H}}}{\hbar}\right] + i\hat{\mathcal{L}}(\hat{S}_{\alpha\beta}) + i\hat{F}_{\alpha\beta}, \tag{4a}$$

$$i\left(\frac{\partial}{\partial z} + \frac{1}{c}\frac{\partial}{\partial t}\right)\hat{E}_{p+} + \frac{g^*_{p+}N}{c}\hat{S}_{14} = 0, \tag{4b}$$

$$i\left(\frac{\partial}{\partial z} + \frac{1}{c}\frac{\partial}{\partial t}\right)\hat{E}_{p-} + \frac{g^*_{p-}N}{c}\hat{S}_{24} = 0. \tag{4c}$$

Here, the damping operator $\hat{\mathcal{L}}$ describes the dissipation process in $\hat{S}_{\alpha\beta}$; $\hat{F}_{\alpha\beta}$ are δ-correlated Langevin noise operators describing the fluctuations associated with the dissipation contributed by $\hat{\mathcal{L}}(\hat{S}_{\alpha\beta})$ [62,63]. The two-time correlation functions of $\hat{F}_{\alpha\beta}$ are defined by $\langle\hat{F}_{\alpha\beta}(z,t)\hat{F}_{\alpha'\beta'}(z',t')\rangle \equiv \mathrm{Tr}_{\mathrm{R}}[\hat{F}_{\alpha\beta}(z,t)\hat{F}_{\alpha'\beta'}(z',t')\hat{\rho}_{\mathrm{R}}]$, where $\hat{\rho}_{\mathrm{R}}$ is the initial density operator of the thermal reservoir coupling to the atomic system and Tr_{R} denotes the trace over the reservoir variables. Explicit expressions of Eq. (4a) are presented in Appendix A.

The model presented above can be realized by realized experiments. One of the candidates is the laser-cooled alkali ^{87}Rb atomic gas with the atomic levels [shown in Fig. 1(a)] assigned to be $|1\rangle = |5^2S_{1/2}, g_{F,1} = -1/2, m_{F,1} = -1\rangle$, $|2\rangle = |5^2S_{1/2}, g_{F,2} = -1/2, m_{F,2} = 1\rangle$, $|3\rangle = |5^2S_{1/2}, g_{F,3} = 1/2, m_{F,3} = 0\rangle$, and $|4\rangle = |5^2P_{1/2}, g_{F,4} = -1/6, m_{F,4} = 0\rangle$ [43], with physical parameters given by $\Gamma_4 = 2\pi\times 5.75$ MHz, $\gamma^{\mathrm{dep}}_{31} = \gamma^{\mathrm{dep}}_{32} \approx 2\pi\times 1$ kHz [64]. If the static magnetic field is chosen to be $B_0 = 1$ G, the Zeeman splitting between sublevels $|1\rangle$ and $|2\rangle$ is $\Delta_2 \equiv \mu_B(g_{F,1}m_{F,1} - g_{F,2}m_{F,2})B_0/\hbar \approx 2\pi\times 1.4$ MHz.

The thermal reservoir coupling to the atomic medium can be safely regarded as a vacuum reservoir $\hat{\rho}_{\mathrm{R}} \approx |\{0\}_{\mathrm{R}}\rangle\langle\{0\}_{\mathrm{R}}|$ [53,54]. This is due to the fact that the excitation energy of signal photons at optical frequency $(\hbar\omega_p)$ is much larger than that of thermal noises of order $k_{\mathrm{B}}T$ (here, k_{B} is the Boltzmann constant and T is temperature) at an ultracold environment, resulting in vanishing thermal noise photons, i.e., $\bar{n}_{\mathrm{th}} \equiv \{\exp[\hbar\omega_p/(k_BT)] - 1\}^{-1} \approx 0$. As a result, all normally ordered two-time correlation functions of the Langevin noise operators are negligible [62,63].

In addition, as suggested in Refs. [52–54], the quantum statistical property (as well as the photon efficiency and quantum-state fidelity) of the signal photon is proportional to the normally ordered correlators of the Langevin noise operators $\hat{F}_{\alpha\beta}$ under the condition of EIT, which is nearly vanishing for the atomic gas at an ultracold environment, as stated before. Therefore the Langevin terms make negligible contributions to the dynamics of photons and are omitted in the following discussion. However, it should be pointed out that special cases should be treated carefully when the Langevin noise terms play significant roles. For example, when one considers the dynamics of some nonclassical optical fields described by continuous variables (such as squeezed vacuum pulses) [30] or when four-wave mixing (FWM) processes (which produce optical gain leading to nonzero populations at excited states) play a significant role, the noise effect cannot be neglected, as studied in Refs. [65–69].

In the absence of the signal field, the steady-state solution of the system is found to be $\hat{S}^{(0)}_{\alpha\beta} = \rho^{(0)}_{11}\delta_{\alpha1}\delta_{\beta1}\hat{I} + \rho^{(0)}_{22}\delta_{\alpha2}\delta_{\beta2}\hat{I}$. Here, $\hat{I}$ is the identity operator; $\rho^{(0)}_{\alpha\alpha}$ $(\alpha = 1,2)$ are initial populations in ground-state sublevels $|1\rangle$ and $|2\rangle$ (with $\rho^{(0)}_{11} + \rho^{(0)}_{22} = 1$), which can be adjusted by, e.g., optical pumping or applying a microwave field coupling to states $|1\rangle$ and $|2\rangle$. Especially, the result of the QM of photons with a single polarization component can be obtained by taking $\rho^{(0)}_{11} = 1$ and $\rho^{(0)}_{22} = 0$. Here, our discussion will focus mainly on the case $\rho^{(0)}_{11} = \rho^{(0)}_{22} = 1/2$.

Because the signal field is much weaker than the control field, the populations in two ground-state sublevels will be kept nearly unchanged when the weak signal field is applied to the atomic gas. In this situation, the HLM equations (4a)–(4c) can be reduced to the form

$$\left(i\frac{\partial}{\partial\tau} + d_{Sj}\right)\hat{\mathcal{S}}_j + \Omega^*_c\hat{\mathcal{P}}_j = 0, \tag{5a}$$

$$\left(i\frac{\partial}{\partial\tau} + d_{Pj}\right)\hat{\mathcal{P}}_j + \Omega_c\hat{\mathcal{S}}_j + \frac{G_p}{\sqrt{2}}\hat{\mathcal{E}}_j = 0, \tag{5b}$$

$$i\frac{\partial}{\partial z}\hat{\mathcal{E}}_j + \frac{G^*_p}{\sqrt{2}c}\hat{\mathcal{P}}_j = 0, \tag{5c}$$

where the subscript j $(=+,-)$ represents the quantities belonging to the σ^+- and σ^--polarized components of the qubit, respectively. In writing Eqs. (5a)–(5c), we have defined $\hat{\mathcal{E}}_\pm = \hat{E}_{p\pm}/\sqrt{L}$, $\hat{\mathcal{P}}_+ = \hat{S}_{14}\sqrt{2N/L}$, $\hat{\mathcal{P}}_- = \hat{S}_{24}\sqrt{2N/L}$, $\hat{\mathcal{S}}_+ = \hat{S}_{13}\sqrt{2N/L}$, and $\hat{\mathcal{S}}_- = \hat{S}_{23}\sqrt{2N/L}$ [70]; moreover, the traveling coordinate $\tau = t - z/c$ is used, and $\Omega_c = \Omega_c(t - z/c) = \Omega_c(\tau)$ is assumed [54]; additionally, for simplified notations, we have defined new parameters $d_{S+} = \Delta_3 + i\gamma_S$, $d_{S-} =$

$\Delta_3 - \Delta_2 + i\gamma_S$, $d_{P+} = \Delta_4 + i\gamma_P$, and $d_{P-} = \Delta_4 - \Delta_2 + i\gamma_P$, with $\gamma_S \equiv \gamma_{31} \approx \gamma_{32}$, $\gamma_P \equiv \gamma_{41} \approx \gamma_{42}$. In Eqs. (5b) and (5c), the quantity G_p ($\equiv g_p\sqrt{N}$) is the coefficient characterizing the collective photon-atom coupling, with $g_p \equiv g_{p+} \approx g_{p-}$ due to the symmetry of the tripod-shaped level configuration.

We are interested in the propagation and QM dynamics of photonic qubits in the system. We assume that at the entrance of the atomic medium ($z = 0$), the signal field is prepared in a state of a single-photon qubit encoded in σ^+- and σ^--polarized components of the signal field, i.e.,

$$|\Psi(0)\rangle \equiv |\Psi(z=0)\rangle = \sqrt{c}\sum_{j=+,-}\int_{-\infty}^{+\infty} d\tau \Psi_{E0j}(\tau)\hat{\mathcal{E}}_j^\dagger(0,\tau)|0\rangle, \quad (6)$$

which obeys the normalization condition $\langle\Psi(0)|\Psi(0)\rangle = \int_{-\infty}^{+\infty} d\tau[|\Psi_{E0+}(\tau)|^2 + |\Psi_{E0-}(\tau)|^2] = 1$. Here, $|0\rangle \equiv |\{0\}_+\rangle|\{0\}_-\rangle$, with $|\{0\}_j\rangle$ being the photon vacuum state of the σ^j-polarized component. $\Psi_{E0j}(\tau)$ is the σ^j-polarized component of the photon wave function (i.e., the probability amplitude for finding the photon in the σ^j-polarized component), assumed to take the Gaussian form

$$\Psi_{E0j}(\tau) = \sqrt{A_j}\Phi_{E0}(\tau), \quad (7a)$$

$$\Phi_{E0}(\tau) = \sqrt{\frac{2\sqrt{\ln(2)}}{t_0\sqrt{\pi}}}\exp\left[-2\ln(2)\frac{\tau^2}{t_0^2}\right], \quad (7b)$$

where t_0 is the FWHM (time duration) of $|\Phi_{E0}(\tau)|^2$ satisfying the normalization condition $\int_{-\infty}^{+\infty} d\tau|\Phi_{E0}(\tau)|^2 = 1$ and $A_j \in [0, 1]$ is the energy fraction of the σ^j-polarized component obeying $A_+ + A_- = 1$.

B. Propagation of single-photon polarization qubits

We first give a brief discussion of the propagation property of the single-photon polarization qubit working under the condition of the double EIT, which will be instructive for the investigation of the QM of single-photon qubits given in the next section.

By taking Ω_c as a constant and employing a Fourier transformation, from the HLM equations (4a)–(4c) we can obtain the propagation solution of the σ^j-polarized component of the signal field

$$\hat{\mathcal{E}}_j(z,\tau) = \frac{1}{\sqrt{2\pi}}\int_{-\infty}^{+\infty} d\omega\tilde{\hat{\mathcal{E}}}_j(0,\omega)e^{i[K_j(\omega)z-\omega\tau]}. \quad (8)$$

Here, K_j is the linear dispersion relation of the σ^j-polarized component given by

$$K_j(\omega) = \frac{|G_p|^2}{2c}\frac{\omega + d_{Sj}}{|\Omega_c|^2 - (\omega + d_{Sj})(\omega + d_{Pj})}. \quad (9)$$

$\hat{\mathcal{N}}_j(z,\tau)$ in the propagation solution (8) is caused by the Langevin noise, with its explicit form shown in Appendix B.

Figure 1(c) shows the linear dispersion relations K_+ and K_- as a function of sideband frequency ω; $\mathrm{Re}(K_j)$ and $\mathrm{Im}(K_j)$ are the real and imaginary parts of K_j ($j = +, -$), respectively. When plotting the figure, the system parameters used were $|G_p|^2/c = 3 \times 10^9\ \mathrm{cm}^{-1}\ \mathrm{s}^{-1}$ corresponding to an atomic density of $\mathcal{N}_a \equiv N/V \approx 1.1 \times 10^{11}\ \mathrm{cm}^{-3}$, $\Omega_c = 3\gamma_P$, $\Delta_3 = 0.25\gamma_P$, and $\Delta_4 = 0.25\gamma_P$, with $2\pi \times 3$ MHz. We see that, in the absorption spectrum of the σ^+-polarized component (σ^--polarized component) characterized by $\mathrm{Im}(K_+)$ (dashed red line) [$\mathrm{Im}(K_-)$ (dashed magenta line)], an EIT transparency window is opened. Since there are two EIT transparency windows opened respectively in the absorption spectra of the two polarization components, the system supports two EITs simultaneously (i.e., the double EIT), induced by a shared control field.

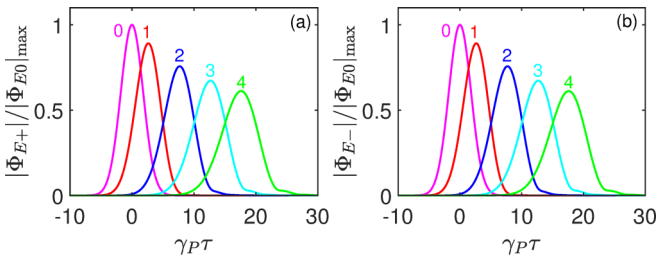

FIG. 2. Propagation of the photon polarization qubit. (a) σ^+-polarized component of the qubit wave function $|\Phi_{E+}|/|\Phi_{E0}|_{\max}$ as a function of nondimensional traveling coordinate $\gamma_P\tau$ ($\gamma_P = 2\pi \times 3$ MHz). Lines 0, 1, 2, 3, and 4 are for $|\Phi_{E+}|/|\Phi_{E0}|_{\max}$ at $z = 0$, $z = 0.25\,L_{\mathrm{disp}}$, $z = 0.75\,L_{\mathrm{disp}}$, $z = 1.25\,L_{\mathrm{disp}}$, and $z = 1.75\,L_{\mathrm{disp}}$, respectively, with $L_{\mathrm{disp}} \approx 2.3$ cm. (b) The same as (a) but for the σ^--polarized component of the qubit wave function $|\Phi_{E-}|/|\Phi_{E0}|_{\max}$.

Dynamics of the polarization qubit can be described by an effective qubit wave function. The σ^j-polarized component of the qubit wave function is defined by

$$\Psi_j(z,\tau) = \langle 0|\hat{\mathcal{E}}_j(z,\tau)|\Psi(0)\rangle, \quad (10)$$

where $|\Psi(0)\rangle$ is given by (6). Shown in Fig. 2 is the qubit wave function during propagation. Figure 2(a) illustrates the wave function of the σ^+-polarized component, i.e., $|\Phi_{E+}|/|\Phi_{E0}|_{\max}$, as a function of nondimensional traveling coordinate $\gamma_P\tau$; lines 0, 1, 2, 3, and 4 are for $|\Phi_{E+}|/|\Phi_{E0}|_{\max}$ at $z = 0$, $z = 0.25\,L_{\mathrm{disp}}$, $z = 0.75\,L_{\mathrm{disp}}$, $z = 1.25\,L_{\mathrm{disp}}$, and $z = 1.75\,L_{\mathrm{disp}}$, respectively, with L_{disp} being the typical dispersion length (see its definition in Appendix B). Figure 2(b) is similar to Fig. 2(a) but for the wave function of the σ^+-polarized component. When plotting the figure, we have chosen $t_0 = 3/\gamma_P$, with other parameters the same as those used in Fig. 1(c), which gives $L_{\mathrm{disp}} \approx 2.3$ cm.

From Fig. 2, we see that the qubit wave function can preserve its shape quite well in a short propagation distance ($z \ll L_{\mathrm{disp}}$), while it undergoes a significant deformation (i.e., the width and amplitude are broadened and lowered, respectively) for a long propagation distance ($z \gg L_{\mathrm{disp}}$). The reasons for the deformation are the following: (i) Due to the coupling with the atoms, the signal field displays a dispersion effect during propagation. (ii) Though the spontaneous emission has been largely suppressed by the quantum interference effect contributed by the double EIT, the decoherences between the bottom levels $|1\rangle$, $|2\rangle$, and $|3\rangle$ of the atoms still cause the absorption of the signal field. For more details, see Appendix B. These propagation characters of the qubit have significant impacts on the performance of the qubit memory; see below.

In addition, the quantum statistical property of the polarization qubit can be described by the intensity correlation functions $g_{\pm}^{(2)}(z,\tau_1,\tau_2)$. It can be shown that $g_{+}^{(2)}(z,\tau_1,\tau_2)\approx g_{-}^{(2)}(z,\tau_1,\tau_2)\approx 0$, which means that, when the system works under the condition of the double EIT, the quantum statistical property of the polarization qubit can be well preserved during propagation. A detailed discussion of the intensity correlation functions $g_{\pm}^{(2)}$ is presented in Appendix B.

III. MEMORY OF SINGLE-PHOTON POLARIZATION QUBITS

A. Analytical results

Now we turn to investigate the memory of the photon polarization qubit based on the HLM equations (5a)–(5c). For simplicity, as in Refs. [30,55] we assume that the time duration of the input qubit wave packet is larger than the inversion of the decay rate of the excited state (i.e., $|t_0 d_{Pj}|>1$). In this situation, the time derivative term $\partial\hat{\mathcal{P}}_j/\partial\tau$ in Eq. (5b) is comparably small and hence can be disregarded, which yields the relation $\hat{\mathcal{P}}_j=-[\Omega_c\hat{\mathcal{S}}_j+(G_p/\sqrt{2})\hat{\mathcal{E}}_j]/d_{Pj}$. With such a consideration, the HLM equations (5a)–(5c) are reduced to

$$\left(i\frac{\partial}{\partial\tau}+d_{Sj}-\frac{|\Omega_c|^2}{d_{Pj}}\right)\hat{\mathcal{S}}_j-\frac{G_p}{\sqrt{2}d_{Pj}}\Omega_c^*\,\hat{\mathcal{E}}_j=0, \quad (11a)$$

$$\left(i\frac{\partial}{\partial z}-\frac{|G_p|^2}{2cd_{Pj}}\right)\hat{\mathcal{E}}_j-\frac{G_p^*}{\sqrt{2}cd_{Pj}}\Omega_c\,\hat{\mathcal{S}}_j=0. \quad (11b)$$

By using a Laplace transformation, the analytical solution of Eqs. (11a) and (11b) can be obtained, with the expression of the signal-field operator $\hat{\mathcal{E}}_j$ $(j=+,-)$ given by

$$\hat{\mathcal{E}}_j(z,\tau)=e^{-\delta_{Pj}D(z)}\hat{\mathcal{E}}_j(0,\tau)+e^{-\delta_{Pj}D(z)}\int_{\tau_0}^{\tau}d\tau' f_j(z,\tau,\tau')\hat{\mathcal{E}}_j(0,\tau'), \quad (12a)$$

$$f_j(z,\tau,\tau')=\frac{\delta_{Pj}}{\gamma_P}\Omega_c(\tau)\Omega_c^*(\tau')e^{id_{Sj}(\tau-\tau')-\kappa_c(\tau,\tau')}\times\sqrt{\frac{\delta_{Pj}D(z)}{\kappa_c(\tau,\tau')}}I_1(2\sqrt{\kappa_c(\tau,\tau')\delta_{Pj}D(z)}). \quad (12b)$$

Here, I_1 is the first-order modified Bessel function; $D(z)\equiv|G_p|^2z/(2c\gamma_P)$ is the optical depth of the signal field in the absence of the control field, estimated by the propagation distance z when the amplitude of the σ^j-polarized component of the signal field decays into $\exp[-D(z)]$ comparing with its input value; and $\kappa_c(\tau_1,\tau_2)\equiv(\delta_{Pj}/\gamma_P)\int_{\tau_2}^{\tau_1}d\tau'|\Omega_c(\tau')|^2$ is a dimensionless quantity, with $\delta_{Pj}\equiv i\gamma_P/d_{Pj}$. A detailed derivation of the solution composed of (12a) and (12b) is presented in Appendix C. Obviously, the solution composed of (12a) and (12b) can be taken as a transformation between the input field operators $\hat{\mathcal{E}}_j(0,\tau)$ and the output field operators $\hat{\mathcal{E}}_j(z,\tau)$. Note that when deriving Eqs. (12a) and (12b), the initial spin waves $\hat{\mathcal{S}}_j(z,\tau_0)$ have been assumed to be zero, which is employed for simplicity and valid for cases where there is no initial coherence between the lower three states, used also by the authors of Refs. [30,54,55].

We now consider the memory of the photon polarization qubit by implementing the time-dependent control field used for the storage and retrieval of the qubit as [71]

$$\Omega_c(\tau)=\frac{\Omega_{cm}}{2}\left[2-\tanh\left(\frac{\tau-T_{\rm off}}{T_s}\right)+\tanh\left(\frac{\tau-T_{\rm on}}{T_s}\right)\right]. \quad (13)$$

Here, Ω_{cm} is the maximum value of Ω_c; $T_{\rm off}$ and $T_{\rm on}$ are the times at which the control field is switched off and on, respectively; the storage time is given by $T_{\rm on}-T_{\rm off}$; and T_s is the duration of the switching time.

The quantum-state fidelity of the memory for the photon polarization qubit is defined by the inner product between the output quantum state $|\Psi(z)\rangle$ and the target quantum state $|\Psi^{\rm tgt}(z)\rangle$ at the propagation distance z, i.e., $F(z)\equiv|\langle\Psi^{\rm tgt}(z)|\Psi(z)\rangle|^2$ [13,72]. Here, $|\Psi(z)\rangle$ is given by

$$|\Psi(z)\rangle=\sqrt{c}\sum_{j=+,-}\int_{T_{\rm on}}^{+\infty}d\tau\,\Psi_{Ej}(z,\tau)\hat{\mathcal{E}}_j^{\dagger}(0,\tau)|0\rangle, \quad (14)$$

where $\Psi_{Ej}(z,\tau)$ is the effective one-photon wave function given by Eq. (10); $|\Psi^{\rm tgt}(z)\rangle$ is given by

$$|\Psi^{\rm tgt}(z)\rangle=\sqrt{c}\sum_{j=+,-}\int_{T_{\rm on}}^{+\infty}d\tau\,\Psi_{Ej}^{\rm tgt}(z,\tau)\hat{\mathcal{E}}_j^{\dagger}(0,\tau)|0\rangle. \quad (15)$$

Note that the lower limit of the above integration is set to be $T_{\rm on}$, which means that one starts to measure the quantum-state fidelity after the control field is switched on. In expression (15), $\Psi_{Ej}^{\rm tgt}(z,\tau)\equiv\Psi_{E0j}(\tau-T_j(z))\exp[i\phi_j(z,\tau)]$ is the target qubit wave packet of the σ^j-polarized component. Here, $\Psi_{E0j}(\tau)$ is the incident qubit wave packet given by Eqs. (7a) and (7b); $T_j(z)$ is the time at which the peak of the σ^j-polarized component of the wave packet locates at the spatial position z (its value is associated with the group delay z/V_{gj}, the switching time T_s, and the storage time $T_{\rm on}-T_{\rm off}$); and $\phi_j(z,\tau)$ is the phase of the qubit wave packet of the σ^j-polarized component $\Psi_{Ej}(z,\tau)$. The values of T_j and ϕ_j are exactly extracted from numerical implementations.

By using Eqs. (14) and (15), we can obtain the explicit expression of the quantum-state fidelity F as a function of the distance z, given by

$$F(z)=\left|\int_{T_{\rm on}}^{+\infty}d\tau[A_+\Phi_{E0}^*(\tau-T_+(z))|\Phi_{E+}(z,\tau)|+A_-\Phi_{E0}^*(\tau-T_-(z))|\Phi_{E-}(z,\tau)|]\right|^2, \quad (16a)$$

$$\Phi_{Ej}(z,\tau)=e^{-\delta_{Pj}D(z)}\Phi_{E0}(\tau)+e^{-\delta_{Pj}D(z)}\int_{\tau_0}^{\tau}d\tau' f_j(z,\tau,\tau')\Phi_{E0}(\tau'). \quad (16b)$$

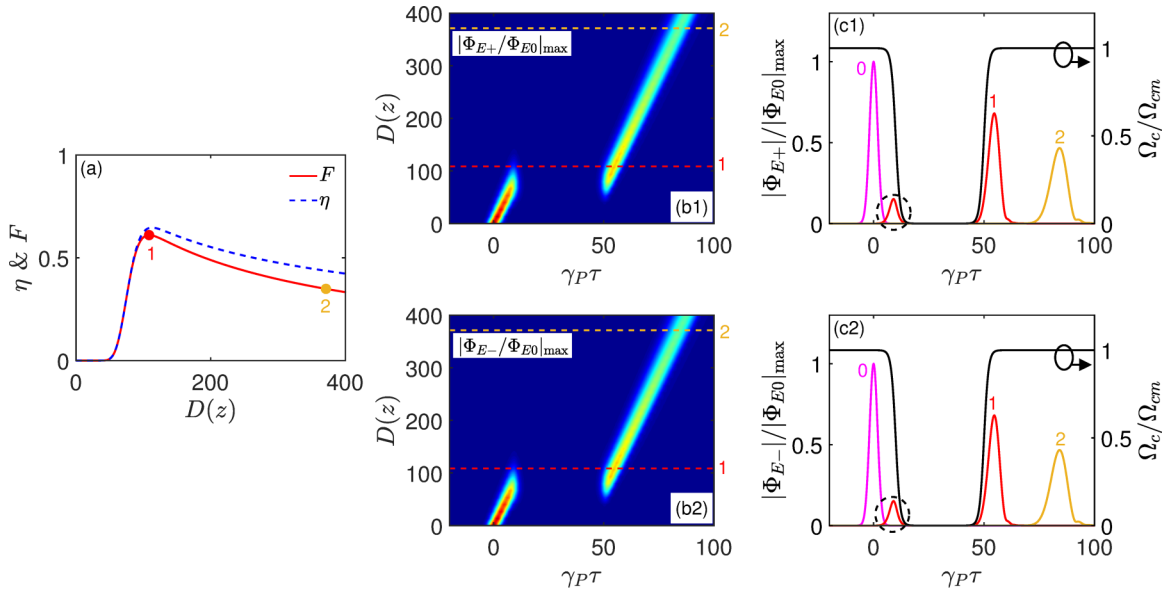

FIG. 3. Storage and retrieval of the single-photon polarization qubit. (a) The efficiency η (dashed blue line) and the quantum-state fidelity F (solid red line) of the qubit memory as functions of optical depth $D = D(z) \equiv |G_p|^2 z/(2c\gamma_P)$. Solid red circle 1 corresponds to the optimal optical depth, i.e., $D = D^{\rm opt} \approx 110$, at which maximum memory efficiency $\eta_{\rm max} \approx 0.71$ and maximum quantum-state fidelity $F_{\rm max} \approx 0.67$ can be obtained almost simultaneously. (b1) Evolution of the modulus of the qubit wave packet of the σ^+-polarized component (i.e., $|\Phi_{E+}|/|\Phi_{E0}|_{\rm max}$) as a function of $\gamma_P\tau$ and D in the process of the qubit memory. The wave packet shown by the bright stripe in the lower left (upper right) is $|\Phi_{E+}|/|\Phi_{E0}|_{\rm max}$ before (after) the storage. (c1) $|\Phi_{E+}|/|\Phi_{E0}|_{\rm max}$ as a function of $\gamma_P\tau$. Solid magenta line 0, $|\Phi_{E+}|/|\Phi_{E0}|_{\rm max}$ for $D = 0$. Solid red line 1, $|\Phi_{E+}|/|\Phi_{E0}|_{\rm max}$ for optimal optical depth $D = D^{\rm opt} \approx 110$, corresponding to solid red circle 1 in (a) and also dashed red line 1 in (b1). Solid orange line 2, $|\Phi_{E+}|/|\Phi_{E0}|_{\rm max}$ for $D \approx 390$, which corresponds to solid orange circle 2 in (a) and also dashed orange line 2 in (b1). (b2) and (c2) are the same as (b1) and (c1), respectively, but for the qubit wave packet of the σ^--polarized component (i.e., $|\Phi_{E-}|/|\Phi_{E0}|_{\rm max}$). Solid black lines in (c1) and (c2) are the half Rabi frequency Ω_c given by Eq. (13), illustrated here to show its switching off and on during the process of the qubit memory. The small solid red curve circled by a dashed black ring in (c1) [(c2)] is the leaky part of $|\Phi_{E+}|/|\Phi_{E0}|_{\rm max}$ ($|\Phi_{E-}|/|\Phi_{E0}|_{\rm max}$) at the optimal optical depth $D^{\rm opt} \approx 110$.

Notice that the *quantum-state fidelity* (16) can be factored as $F(z) = \eta(z)J^2(z)$ [13]. Here, $\eta(z)$ is the photon *memory efficiency* defined as the energy ratio between the total output and the input photons in the signal field, given by [13,54,55]

$$\begin{aligned}\eta(z) &= \frac{\int_{T_{\rm on}}^{+\infty} d\tau[\langle\Psi(0)|\hat{\mathcal{E}}_+^\dagger(z,\tau)\hat{\mathcal{E}}_+(z,\tau)|\Psi(0)\rangle + \langle\Psi(0)|\hat{\mathcal{E}}_-^\dagger(z,\tau)\hat{\mathcal{E}}_-(z,\tau)|\Psi(0)\rangle]}{\int_{\tau_0}^{T_{\rm off}} d\tau[\langle\Psi(0)|\hat{\mathcal{E}}_+^\dagger(0,\tau)\hat{\mathcal{E}}_+(0,\tau)|\Psi(0)\rangle + \langle\Psi(0)|\hat{\mathcal{E}}_-^\dagger(0,\tau)\hat{\mathcal{E}}_-(0,\tau)|\Psi(0)\rangle]} \\ &= \int_{T_{\rm on}}^{+\infty} d\tau[A_+|\Phi_{E+}(z,\tau)|^2 + A_-|\Phi_{E-}(z,\tau)|^2]; \end{aligned} \tag{17}$$

$J^2(z)$ is the *wave-shape similarity* between the output and the target qubit wave packets, defined in the form of the Cauchy-Schwarz inequality [13,72]

$$J^2(z) = \frac{\left|\int_{T_{\rm on}}^{+\infty} d\tau[A_+\Phi_{E0}^*(\tau - T_+(z))|\Phi_{E+}(z,\tau)| + A_-\Phi_{E0}^*(\tau - T_-(z))|\Phi_{E-}(z,\tau)|]\right|^2}{\int_{T_{\rm on}}^{+\infty} d\tau[A_+|\Phi_{E+}(z,\tau)|^2 + A_-|\Phi_{E-}(z,\tau)|^2]}, \tag{18}$$

which is smaller than or equal to 1 [$J^2 = 1$ is achieved only when $\Phi_{E+}(z,\tau) = \Phi_{E0}(\tau - T_+(z))$ and $\Phi_{E-}(z,\tau) = \Phi_{E0}(\tau - T_-(z))$ are both exactly achieved]. In writing Eqs. (17) and (18), we have used the normalization condition of the input qubit wave functions $(A_+ + A_-)\int_{\tau_0}^{T_{\rm off}} d\tau|\Phi_{E0}(\tau)|^2 = 1$. From the above results one sees that the quantum-state fidelity F for the single-photon qubit memory is determined by two factors. One is the memory efficiency η, which is largely related by the optical absorption (energy loss) of the photon during the storage and retrieval, caused by the decoherence of the system; the other one is the wave-shape similarity J^2, which is largely determined by the dispersion of the qubit wave packet during propagation.

B. Numerical results

Based on the above analytical analysis, we now carry out numerical calculations on the memory of the photon polarization qubit in the system via double EIT, with the results summarized in Fig. 3. The physical parameters used in

the numerical calculations are $\Omega_{cm} = 3\gamma_P$, $t_0 = 3/\gamma_P$, $A_+ = A_- = 1/2$, $T_{\rm off} = 10/\gamma_P$, $T_{\rm on} = 50/\gamma_P$, and $T_s = 2/\gamma_P$ ($\gamma_P = 2\pi \times 3$ MHz), with the other parameters being the same as those used in Fig. 1(c).

Shown in Fig. 3(a) are the efficiency η and the quantum-state fidelity F of the qubit memory, plotted by the dashed blue and solid red lines, respectively, and both of them are taken to be functions of optical depth $D = D(z) \equiv |G_p|^2 z/(2c\gamma_P)$. From the figure, we can obtain the following conclusions: (i) Both the efficiency η and the fidelity F grow first as the optical depth D increases; then they arrive at their maxima and finally decay as D increases further. (ii) There exists an optimal optical depth, i.e., $D = D^{\rm opt} \approx 110$, at which one can acquire maximum memory efficiency $\eta_{\rm max} = 0.71$ and maximum fidelity $F_{\rm max} \approx 0.67$ almost simultaneously [73]. The reasons for the appearance of such behaviors can be explained as follows: In the process of the storage and retrieval of the qubit wave packet, for small propagation distance (i.e., $D < D^{\rm opt}$) the effects of the dispersion and absorption of the system are negligible, and hence η and F grow as D increases; however, for large distance (i.e., $D > D^{\rm opt}$) the effects of the dispersion and absorption play significant roles, and hence η and F are reduced as D becomes larger.

In order to gain deep insight into the dynamics of the qubit memory, the evolution of the qubit wave packets of the two polarization components of the signal field is numerically simulated, with the results shown in the remaining four panels of Fig. 3. The system parameters used in the simulation are chosen to be the same as those used in Fig. 3(a).

Illustrated in Fig. 3(b1) is the evolution of the modulus of the qubit wave packet of the σ^+-polarized component (i.e., $|\Phi_{E+}|/|\Phi_{E0}|_{\rm max}$) as a function of $\gamma_P\tau$ and D in the process of the qubit memory. The qubit wave packet (shown by the bright stripe) given in the lower left (upper right) is $|\Phi_{E+}|/|\Phi_{E0}|_{\rm max}$ before (after) the storage. Figure 3(c1) shows the wave shape of $|\Phi_{E+}|/|\Phi_{E0}|_{\rm max}$ as a function of $\gamma_P\tau$ for different optical depths D. Solid magenta line 0 is for $D = 0$; solid red line 1 is for $D \approx 110$ (optimal optical depth), which corresponds to solid red circle 1 in Fig. 3(a) and also dashed red line 1 in Fig. 3(b1). Solid orange line 2 is for $D \approx 390$, which corresponds to solid orange circle 2 in Fig. 3(a) and also dashed orange line 2 in Fig. 3(b1).

Figures 3(b2) and 3(c2) are the same as Figs. 3(b1) and 3(c1), respectively, but for the qubit wave packet of the σ^--polarized component (i.e., $|\Phi_{E-}|/|\Phi_{E0}|_{\rm max}$). For completeness, in Figs. 3(c1) and 3(c2) we have also depicted by solid black lines the half Rabi frequency of the control field Ω_c [given by Eq. (13)] as a function of τ, illustrating clearly the process of the switching off and on of the control field during the qubit memory. The small solid red line circled by a dashed black ring in Fig. 3(c1) [Fig. 3(c2)] represents the leaky part of $|\Phi_{E+}|/|\Phi_{E0}|_{\rm max}$ ($|\Phi_{E-}|/|\Phi_{E0}|_{\rm max}$) at the optimal optical depth $D^{\rm opt} \approx 110$.

From the results given in Figs. 3(b1), 3(b2), 3(c1), and 3(c2), we can see that the qubit memory is realized in the following way: (i) Before the storage of the qubit, the control field is switched on; the input qubit wave packets of both the σ^+- and σ^--polarized components propagate freely in the atomic medium. (ii) When the control field is switched off at $t = T_{\rm off}$, two qubit wave-packet components [i.e., solid magenta line 0 in Figs. 3(c1) and 3(c2)] are adiabatically stored into the atomic medium; lately, when the control field is switched on again at $t = T_{\rm on}$, two qubit wave-packet components are retrieved, which can acquire maximal memory efficiency $\eta_{\rm max}$ and maximum fidelity $F_{\rm max}$ at the optimal optical depth $D^{\rm opt}$ [see solid red line 1 in Figs. 3(c1) and 3(c2)]. (iii) When the propagation distance is increased to make the optical depth larger than the optimal one, the two qubit wave-packet components [i.e., solid yellow line 2 in Figs. 3(c1) and 3(c2)] undergo some deformations, i.e., their widths are increased and their amplitudes are lowered (caused by the dispersion and absorption of the system), which brings a reduction of the efficiency and fidelity of the qubit memory. From the figure, one can also see that there is a high symmetry for the memory processes between Fig. 3(b1) and Fig. 3(b2) [also between Fig. 3(c1) and Fig. 3(c2)]. This is due to the fact that the tripod atomic level configuration [Fig. 1(a)] and the input condition composed of (7a) and (7b) chosen here are highly symmetric for the σ^+- and σ^--polarized components of the qubit.

C. Optimization of the single-photon qubit memory

The maximum efficiency $\eta_{\rm max}$, the fidelity $F_{\rm max}$, and their corresponding optimal optical depths $D^{\rm opt}$ for the qubit memory can be optimized by suppressing the dispersion and absorption effects of the qubit wave-packet components through the choice of system parameters. To demonstrate this, as an example we fix most system parameters used in Fig. 3 but take t_0 [the time duration of the input qubit pulse; see (7a) and (7b)] and Ω_{cm} [the maximum half Rabi frequency of the control field; see (13)] as two optimization parameters, which are easily implemented experimentally.

Firstly, we fix $\Omega_{cm} = 3\gamma_P$ ($\gamma_P = 2\pi \times 3$ MHz) and study the dependence of $\eta_{\rm max}$, $F_{\rm max}$, and $D^{\rm opt}$ on the nondimensional input time duration of the qubit pulse, i.e., t_0, with the numerical result given in Fig. 4(a1). In the figure, circle-marked dashed blue and circle-marked solid red lines are $\eta_{\rm max}$ and $F_{\rm max}$, respectively; triangle-marked dashed blue and solid red lines are the corresponding $D^{\rm opt}$ for $\eta_{\rm max}$ and $F_{\rm max}$, respectively. We see that both $F_{\rm max}$ and $\eta_{\rm max}$ arise when t_0 increases; then they reach a stationary maximum value of $\eta_{\rm max} \approx F_{\rm max} \approx 0.72$ and keep this value nearly invariant as t_0 is increased further. The physical reason for such behavior is the following: As t_0 increases, the frequency bandwidth of the qubit pulse (proportional to t_0^{-1}) is reduced; hence the sideband absorption and the dispersion effect of the qubit pulse are reduced, which results in the increase in the memory efficiency $\eta_{\rm max}$ and fidelity $F_{\rm max}$.

Drawn in Fig. 4(a2) is the numerical result of the qubit memory for $\Omega_{cm} = 3\,\gamma_P$ and $t_0 = 6.6/\gamma_P$, where the solid red line and the dashed blue line on the right-hand side are the retrieved qubit wave packets of the σ^+- and σ^--polarized components, respectively, at the optimal optical depth $D^{\rm opt} \approx 135$ [74]. Note that, due to the symmetry of the tripod level configuration, the retrieved two polarization components have closed wave shape and travel with closed group velocity, and they coincide with each other in space. The solid black curve shows the switching off and on of the control field Ω_c during the memory process. One sees that the dispersion effect of

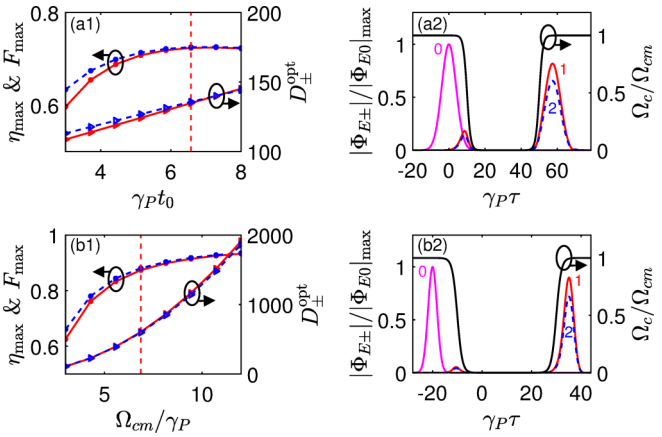

FIG. 4. (a1) Maximum memory efficiency $\eta_{\max}$ (circle-marked dashed blue line) and fidelity $F_{\max}$ (circle-marked solid red line) and their corresponding optimal optical depths $D^{\rm opt}$ (triangle-marked dashed blue and solid red lines, respectively) as functions of $\gamma_P t_0$ for $\Omega_{cm} = 3\gamma_P$. (a2) Right part: optimized retrievals of the qubit pulse for the σ^+-polarized (solid red line 1) and σ^--polarized (dashed blue line 2) components [74] at the optimal optical depth $D^{\rm opt} \approx 135$ as functions of $\gamma_P\tau$ for $\Omega_{cm} = 3\gamma_P$ and $t_0 = 6.6/\gamma_P$, giving rise to $F_{\max} \approx \eta_{\max} \approx 0.72$ [corresponding to the dashed red line in (a1)]. Left part: the small solid red and dashed blue curves are leaked qubit components of the retrieved qubit pulse. (b1) Maximum memory efficiency $\eta_{\max}$ (circle-marked dashed blue line) and fidelity $F_{\max}$ (circle-marked solid red line) and their corresponding optimal optical depths $D^{\rm opt}$ (triangle-marked solid red and dashed blue lines, respectively) as functions of Ω_{cm}/γ_P for $t_0 = 3/\gamma_P$. (b2) Optimized retrievals of the wave packets of the σ^+-polarized (solid red line 1) and σ^--polarized (dashed blue line 2) components [74] at the optimal optical depth $D^{\rm opt} \approx 580$ as functions of $\gamma_P\tau$ for $t_0 = 3/\gamma_P$ and $\Omega_{cm} = 6.8\gamma_P$, giving rise to $F_{\max} \approx \eta_{\max} \approx 0.88$ [corresponding to the dashed red line in (b1)]. Solid magenta curve 0 in (a2) and (b2) denotes the incident qubit wave packets (corresponding to $D = 0$; its two components have been chosen to have the same wave shape and hence coincided).

the system is suppressed in the retrieved qubit pulse. This is different from the results given in Figs. 3(c1) and 3(c2), where $\Omega_{cm} = 3\gamma_P$ and $t_0 = 3/\gamma_P$ and hence the dispersion effect (efficiency and fidelity) is larger (smaller) than the case discussed here.

Secondly, we fix $t_0 = 3/\gamma_P$ and study the dependence of $\eta_{\max}$, $F_{\max}$, and their corresponding optimal optical depths $D^{\rm opt}$ on the maximum half Rabi frequency of the control field, i.e., Ω_{cm}, with the result given in Fig. 4(b1). From the figure we see that as Ω_{cm} is increased, both $F_{\max}$ and $\eta_{\max}$ increase, and $F_{\max}$ gradually coincides with $\eta_{\max}$ for large Ω_{cm}. The physical reasons for such a property can be understood in the following: (i) The increase in the control field enlarges both transparency windows of the double EIT and thus brings the increase in the typical absorption length of the system; see Appendix B). This means that the optical absorption of the qubit pulse due to the spontaneous emission of the atoms is further suppressed, resulting in an increase in the memory efficiency η. (ii) When Ω_{cm} arises, the typical dispersion length of the system, i.e., $L_{\rm disp}$, also arises, which means that the dispersion effect of the qubit pulse is reduced and hence the wave-shape similarity J^2 is increased. Consequently, the quantum-state fidelity F of the qubit memory is enlarged.

Figure 4(b2) shows the numerical result of the qubit memory for $\Omega_{cm} = 6.8\,\gamma_P$ and $t_0 = 3/\gamma_P$, in which the solid red and the dashed blue lines on the right-hand side are the retrieved qubit wave packets of the σ^+- and σ^--polarized components, respectively (these two wave packets also coincide in space) at the optimal optical depth $D^{\rm opt} \approx 580$, yielding $\eta_{\max} \approx F_{\max} \approx 0.88$. We see that the absorption and the dispersion effect of the qubit pulse are significantly lowered and its leaky part is very little compared with those shown in Figs. 3(c1) and 3(c2) for $\Omega_{cm} = 3\gamma_P$ and $t_0 = 3/\gamma_P$, where both the absorption and the dispersion (the efficiency and fidelity) are larger (smaller) than the case considered here, which agrees with the recent experimental observation on the qubit memory reported in Ref. [51].

Based on the above results, we see that the efficiency and fidelity of the qubit memory can arise indeed through the increase in the time duration of the input pulse and the control-field intensity. Additionally, the curves shown in the lower parts of Figs. 4(a1) and 4(b1) also indicate that higher $F_{\max}$ and $\eta_{\max}$ are usually accompanied by larger optimal optical depth $D^{\rm opt}$, which is in agreement with previous theoretical [52–54] and experimental [75] studies for the photon storage with only one polarization component.

IV. QUANTUM MEMORY OF SINGLE-PHOTON QUDITS

The theoretical scheme of the photon qubit memory developed above can be generalized to the memory of photon qudits, multicomponent counterparts of photon qubits useful for increasing information-carrying capacity [7,76]. Shown in Fig. 5(a) is the energy-level diagram and excitation scheme of an $(N+1)$-pod atomic system allowing the memory of photons encoded in N degrees of freedom, where one control field (with amplitude $\mathcal{E}_c$) drives the transition $|N+1\rangle \leftrightarrow |N+2\rangle$ and the jth component of the signal field [with photon annihilation operator $\hat{\mathcal{E}}_j$ $(j = 1, \ldots, N)$] drives the transition $|j\rangle \leftrightarrow |N+2\rangle$, with Δ_j being the detuning and Γ being the spontaneous emission from the excited state $|N+2\rangle$.

Similar to Eq. (6), the incident quantum state for the single-photon qudit of the signal field is assumed to be

$$|\Psi\rangle = \sqrt{c}\sum_{j=1}^{N}\left[\sqrt{A_j}\int_{-\infty}^{+\infty} d\tau\,\Phi_{E0}(\tau)\hat{\mathcal{E}}_j^{\dagger}(0,\tau)\right]|0\rangle, \quad (19)$$

where $\Phi_{E0}(\tau)$ is given by Eqs. (7a) and (7b); A_j are the amplitudes of the jth components obeying the normalization condition $\sum_{j=1}^{N} A_j = 1$.

We focus on the case that the atoms are initially prepared to have equal populations at the ground-state sublevels $|j\rangle$ $(j = 1, \ldots, N)$, i.e., $\rho_{jj}^{(0)} = 1/N$. Then the optical depths for each of the components are identical, defined by $D(z) \equiv |G_p|^2 z/(Nc\gamma_P)$. The derivation of the quantum-state fidelity of qudit memory is similar to that of the qubit memory, with the

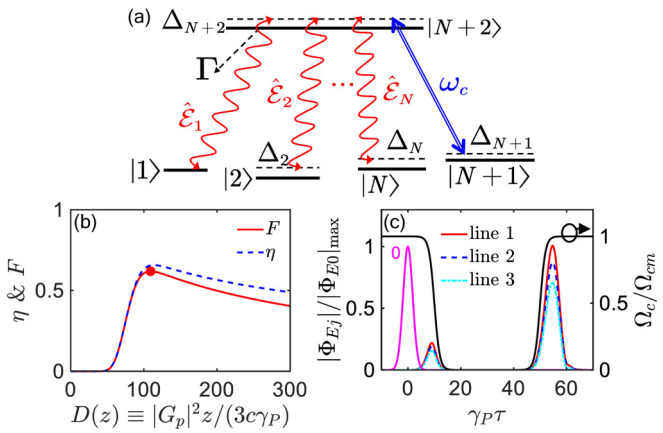

FIG. 5. (a) Energy-level diagram and excitation scheme of an $(N+1)$-pod atomic system. $\hat{\mathcal{E}}_j$ $(j=1,\ldots,N)$ is the photon annihilation operator of the jth component coupling with the atomic transition $|j\rangle \leftrightarrow |N+2\rangle$; the control field with amplitude $\mathcal{E}_c$ drives the transition $|N+1\rangle \leftrightarrow |N+2\rangle$. (b) The efficiency η (dashed blue line) and the fidelity F (solid red line) of the memory of a single-photon qudit as a function of the optical depth $D = D(z) \equiv |G_p|^2 Nz/(3c\gamma_P)$ for $N = 3$. The solid red circle denotes the position $D = D^{\rm opt} \approx 110$ for achieving the maximum fidelity $F_{\max} \approx 0.62$. (c) Right part: $|\Phi_{Ej}|/|\Phi_{E0}|_{\max}$ $(j = 1, 2, 3)$ as functions of $\gamma_P\tau$ retrieved at optimal optical depth $D = D^{\rm opt} \approx 110$ [corresponding to the solid red circle in (b)]. Solid red line 1 is for $|\Phi_{E1}|/|\Phi_{E0}|_{\max}$ at an optimal optical depth $D = D^{\rm opt} \approx 110$; dashed blue line 2 is the same as solid red line 1, but for $|\Phi_{E2}|/|\Phi_{E0}|_{\max}$; dash-dotted cyan line 3 is the same as solid red line 1, but for $|\Phi_{E3}|/|\Phi_{E0}|_{\max}$ [77]. Left part: solid magenta curve 0 is the input qudit pulse (corresponding to $D = 0$; its three components have been chosen to have the same wave shape and hence coincided); the small solid red, dashed blue, and dash-dotted cyan curves are leaked qudit components of the retrieved qudit pulse. The solid black line in the figure is the half Rabi frequency Ω_c given by Eq. (13).

result given by

$$F(z) = \left| \sum_{j=1}^{N} \left[A_j \int_{T_{\rm on}}^{+\infty} d\tau \Phi_{E0}^*(\tau - T_j(z)) |\Phi_{Ej}(z,\tau)| \right] \right|^2. \tag{20}$$

Here, $T_j(z)$ is the time at which the peak of the jth component of the qubit wave packet locates at the spatial position z, which is exactly extracted by numerical implementation. $\Phi_{Ej}(z,\tau)$ is formally given by Eq. (16b), but with $\delta_{Pj} = i\gamma_P/d_{Pj}$ and $d_{Pj} = \Delta_{N+2} - \Delta_j + i\gamma_P$. Similar to Eq. (17), the qudit memory efficiency is given by

$$\eta(z) = \sum_{j=1}^{N} \left[A_j \int_{T_{\rm on}}^{+\infty} d\tau |\Phi_{Ej}(z,\tau)|^2 \right]. \tag{21}$$

As an example, here we consider the case of the qudit memory with $N = 3$. The atoms are chosen to be the laser-cooled alkali ^{87}Rb atomic gas with the atomic levels [see Fig. 5(a)] assigned to be $|1\rangle = |5^2S_{1/2}, g_{F,1} = -1/2, m_{F,1} = -1\rangle$, $|2\rangle = |5^2S_{1/2}, g_{F,2} = -1/2, m_{F,2} = 1\rangle$, $|3\rangle = |5^2S_{1/2}, g_{F,3} = -1/2, m_{F,3} = 0\rangle$, $|4\rangle = |5^2S_{1/2}, g_{F,4} = 1/2, m_{F,4} = 0\rangle$, and $|5\rangle = |5^2P_{1/2}, g_{F,5} = -1/6, m_{F,5} = 0\rangle$, with parameters $\gamma_P \equiv \gamma_{51} \approx \gamma_{52} \approx \gamma_{53} = \Gamma/2 = 2\pi \times 3$ MHz [64]. To satisfy transition selection rules, the control field driving the transition $|4\rangle \leftrightarrow |5\rangle$ should be linearly polarized; the three components of the signal field that drive the transitions $|1\rangle \leftrightarrow |5\rangle$, $|2\rangle \leftrightarrow |5\rangle$, and $|3\rangle \leftrightarrow |5\rangle$ should be chosen to be right polarized, linearly polarized, and left polarized, respectively. The static magnetic field is chosen to be $B_0 = 1$ G; thus $\Delta_2 \equiv \mu_B(g_{F,1}m_{F,1} - g_{F,2}m_{F,2})B_0/\hbar \approx 2\pi \times 1.4$ MHz and $\Delta_3 \equiv \mu_B(g_{F,1}m_{F,1} - g_{F,3}m_{F,3})B_0/\hbar \approx 2\pi \times 0.7$ MHz.

Based on Eqs. (20) and (21), we perform numerical simulations on the memory of the single-photon qudit by using $\Delta_4 = \Delta_5 = 0.5\gamma_P$, $A_1 = A_2 = A_3 = 1/3$, with other physical parameters the same those used in Fig. 3. The results for the efficiency η and fidelity F as functions of the optical depth $D = D(z) \equiv |G_p|^2 z/(3c\gamma_P)$ are shown in Fig. 5(b). Similar to the qubit memory with the corresponding result shown in Fig. 3(a), the maximum efficiency $\eta_{\max} \approx 0.66$ and the maximum fidelity $F_{\max} \approx 0.62$ can be acquired almost simultaneously at the optimal optical depth $D^{\rm opt} \approx 109$. Modules of the three components of the qudit pulse at the optimal optical depth are shown in Fig. 5(c) [77], from which one sees that, similar to the corresponding results given in Figs. 3(c1) and 3(c2) for the qubit memory, all three qudit components can be optimally retrieved at the optimal optical depth by which the maximum memory efficiency and fidelity can be realized (see the description given in the caption of Fig. 5).

V. SUMMARY

In this paper, we have presented a theoretical study on QMs by considering the storage and retrieval of single-photon polarization qubits in a tripod-shaped atomic gas working under a double EIT, in which the storage efficiency and the quantum-state fidelity of the qubit memory are both calculated. We have shown that the optimal optical depth for acquiring the maximum efficiency $\eta_{\max}$ and maximum fidelity $F_{\max}$ of the qubit memory can be acquired simultaneously, which can be further improved by suppressing the optical absorption and dispersion via the choice of the time duration of the input qubit pulse and the amplitude of the control field. In addition, we have estimated the improved efficiency and fidelity of the QM for single-photon qudits. The results reported here are useful for understanding the quantum transmission property of multicomponent slow lights. The theoretical method can be generalized to study the QM of photons with multiple spatial modes (e.g., orbital angular momentum states of single photons) and photons with entanglements. They are also helpful for guiding new experimental findings of high-quality memory of photons.

ACKNOWLEDGMENTS

This work was supported by the National Natural Science Foundation of China under Grant No. 11975098 and the research funds of Flower of Happiness, ECNU, under Grant No. 2020ECNU-XFZH005.

APPENDIX A: EXPLICIT EXPRESSIONS OF THE HEISENBERG-LANGEVIN EQUATIONS

Explicit expression of the Heisenberg-Langevin equation (4a) is given by

$$i\frac{\partial}{\partial t}\hat{S}_{11} - i\Gamma_{14}\hat{S}_{44} + g_{p+}^{*}\hat{E}_{p+}^{\dagger}\hat{S}_{14} - g_{p+}\hat{S}_{41}\hat{E}_{p+} - i\hat{F}_{11} = 0, \tag{A1a}$$

$$i\frac{\partial}{\partial t}\hat{S}_{22} - i\Gamma_{24}\hat{S}_{44} + g_{p-}^{*}\hat{E}_{p-}^{\dagger}\hat{S}_{24} - g_{p-}\hat{S}_{42}\hat{E}_{p-} - i\hat{F}_{22} = 0, \tag{A1b}$$

$$i\frac{\partial}{\partial t}\hat{S}_{33} - i\Gamma_{34}\hat{S}_{44} + \Omega_{c}^{*}\hat{S}_{34} - \Omega_{c}\hat{S}_{43} - i\hat{F}_{33} = 0, \tag{A1c}$$

$$i\left(\frac{\partial}{\partial t} + \Gamma_4\right)\hat{S}_{44} - \Omega_{c}^{*}\hat{S}_{34} + \Omega_{c}\hat{S}_{43} - g_{p+}^{*}\hat{E}_{p+}^{\dagger}\hat{S}_{14} + g_{p+}\hat{S}_{41}\hat{E}_{p+} - g_{p-}^{*}\hat{E}_{p-}^{\dagger}\hat{S}_{24} + g_{p-}\hat{S}_{42}\hat{E}_{p-} - i\hat{F}_{44} = 0, \tag{A1d}$$

$$\left(i\frac{\partial}{\partial t} + d_{21}\right)\hat{S}_{12} + g_{p-}^{*}\hat{E}_{p-}^{\dagger}\hat{S}_{14} - g_{p+}\hat{S}_{42}\hat{E}_{p+} - i\hat{F}_{12} = 0, \tag{A1e}$$

$$\left(i\frac{\partial}{\partial t} + d_{43}\right)\hat{S}_{34} + \Omega_{c}(\hat{S}_{33} - \hat{S}_{44}) + g_{p1+}\hat{S}_{31}\hat{E}_{p+} + g_{p-}\hat{S}_{32}\hat{E}_{p-} - i\hat{F}_{34} = 0, \tag{A1f}$$

$$\left(i\frac{\partial}{\partial t} + d_{31}\right)\hat{S}_{13} + \Omega_{c}^{*}\hat{S}_{14} - g_{p+}\hat{S}_{43}\hat{E}_{p+} - i\hat{F}_{13} = 0, \tag{A1g}$$

$$\left(i\frac{\partial}{\partial t} + d_{32}\right)\hat{S}_{23} + \Omega_{c}^{*}\hat{S}_{24} - g_{p-}\hat{S}_{43}\hat{E}_{p-} - i\hat{F}_{23} = 0, \tag{A1h}$$

$$\left(i\frac{\partial}{\partial t} + d_{41}\right)\hat{S}_{14} + \Omega_{c}\hat{S}_{13} + g_{p+}(\hat{S}_{11} - \hat{S}_{44})\hat{E}_{p+} + g_{p-}\hat{S}_{12}\hat{E}_{p-} - i\hat{F}_{14} = 0, \tag{A1i}$$

$$\left(i\frac{\partial}{\partial t} + d_{42}\right)\hat{S}_{24} + \Omega_{c}\hat{S}_{23} + g_{p-}(\hat{S}_{22} - \hat{S}_{44})\hat{E}_{p-} + g_{p+}\hat{S}_{21}\hat{E}_{p+} - i\hat{F}_{24} = 0. \tag{A1j}$$

Here, $d_{\alpha\beta} = \Delta_\alpha - \Delta_\beta + i\gamma_{\alpha\beta}$ $(\alpha \neq \beta)$ with $\gamma_{\alpha\beta} \equiv (\Gamma_\alpha + \Gamma_\beta)/2 + \gamma_{\alpha\beta}^{\rm dep}$, where $\Gamma_1 = \Gamma_2 = \Gamma_3 \equiv 0$, and $\Gamma_4 \equiv \Gamma_{14} + \Gamma_{24} + \Gamma_{34}$, with $\Gamma_{\alpha\beta}$ being the decay rate of the spontaneous emission from the state $|\beta\rangle$ to the state $|\alpha\rangle$ and $\gamma_{\alpha\beta}^{\rm dep}$ being the dephasing rate between $|\alpha\rangle$ and $|\beta\rangle$.

APPENDIX B: ANALYTICAL RESULTS ON THE QUANTUM STATISTICAL PROPERTY AND THE PROPAGATION OF THE PHOTON POLARIZATION QUBIT

Here, we give a detailed analysis of the quantum statistical and propagating properties of the photon polarization qubit. The quantum statistical property of the photon polarization qubit is characterized by the intensity correlation functions $g_{\pm}^{(2)}(z,\tau_1,\tau_2) = G_{\pm}^{(2)}(z,\tau_1,\tau_2)/[I_{\pm}(z,\tau_1)I_{\pm}(z,\tau_2)]$, quantifying the joint probability of detecting one photon at the position z and time τ_1 and a second photon at the same position z and time τ_2. Here, $G_{\pm}^{(2)}(z,\tau_1,\tau_2) \equiv c^2\langle\Psi(0)|\hat{\mathcal{E}}_{\pm}^{\dagger}(z,\tau_1)\hat{\mathcal{E}}_{\pm}^{\dagger}(z,\tau_2)\hat{\mathcal{E}}_{\pm}(z,\tau_2)\hat{\mathcal{E}}_{\pm}(z,\tau_1)|\Psi(0)\rangle$ is the Glauber two-photon correlation function, and $I_{\pm}(z,\tau) = \langle\Psi(0)|\hat{\mathcal{E}}_{\pm}^{\dagger}(z,\tau)\hat{\mathcal{E}}_{\pm}(z,\tau)|\Psi(0)\rangle$ is the light intensity of the σ^j-polarized component of the qubit $(j = +,-)$. With the input condition (6), we immediately obtain $G_{\pm}^{(2)}(z,\tau_1,\tau_2) \approx 0$. Therefore the intensity correlation functions $g_{+}^{(2)}(z,\tau_1,\tau_2) \approx g_{-}^{(2)}(z,\tau_1,\tau_2) \approx 0$, which means that the quantum statistical property of the photon polarization qubit can be well preserved under the condition of EIT.

To see the absorption and dispersion properties of the qubit pulse, we seek an approximated analytical expression of the effective wave function [78] of the qubit, defined by [also see Eq. (10)]

$$\Psi_j(z,\tau) = \langle 0|\hat{\mathcal{E}}_j(z,\tau)|\Psi(0)\rangle. \tag{B1}$$

Using the result of $\hat{\mathcal{E}}_j(z,\tau)$ and making the Taylor expansion on $K_j(\omega)$ around $\omega = 0$, we obtain

$$\Psi_j(z,\tau) \approx \sqrt{A_j}\Phi_{Ej}(z,\tau), \tag{B2a}$$

$$\Phi_{Ej}(z,\tau) \approx \sqrt{\frac{2\sqrt{\ln(2)}}{t_0\beta_j(z)\sqrt{\pi}}}\exp\left(-\frac{z}{L_{{\rm A},j}}\right) \times \exp\left[-\frac{2\ln(2)}{t_0^2\beta_j(z)}\left(\tau - \frac{z}{V_{gj}}\right)^2\right], \tag{B2b}$$

$$L_{{\rm A},j} \equiv \left[{\rm Im}\left(\frac{d_{3j}}{|\Omega_c|^2 - d_{3j}d_{4j}}\right)\right]^{-1}, \qquad \beta_j(z) \equiv 1 - i\frac{z}{L_{{\rm disp},j}}. \tag{B2c}$$

Here, $V_{gj} \equiv (\partial K_j/\partial\omega)^{-1}|_{\omega=0}$ is the group velocity of the σ^j-polarized component; $L_{{\rm A},j}$ and $L_{{\rm disp},j} \equiv t_0^2/[4\ln(2)K_{2j}]$ are typical absorption and dispersion lengths, respectively, of the σ^j-polarized component, with $K_{2j} \equiv (\partial^2 K_j/\partial\omega^2)^{-1}|_{\omega=0}$. Due to the (tripod) symmetry of the system, $K_2 \approx K_1 \equiv K$, $V_{g2} \approx V_{g1}$, $K_{22} \approx K_{21}$, and hence $L_{{\rm disp},2} \approx L_{{\rm disp},1} \equiv L_{\rm disp}$, $L_{{\rm A},2} \approx L_{{\rm A},1} \equiv L_{\rm A}$, $\beta_2(z) \approx \beta_1(z)$.

Although a large dispersion can lead to a slowdown of the group velocity (i.e., slow light) under the condition of EIT, the large dispersion also can result in a significant deformation of the qubit wave packet and hence the degradation of the

quantum-state fidelity of qubit memory at the propagation distance z comparable to the typical dispersion length $L_{\rm disp}$. Therefore there is a trade-off between the slowdown of the qubit wave packet during the storage by increasing the dispersion and the improvement in the quantum-state fidelity for the retrieved qubit wave packet by suppressing the dispersion. To optimize the quality of the qubit memory, we can tune the values of the dispersion and absorption lengths through selecting the values of Ω_c and t_0. The increase in Ω_c and t_0 results in an enlargement of the dispersion and absorption lengths; in this case the qubit pulse can maintain its waveform for longer propagation distance. With the system parameters given in Sec. II B, we have $L_{\rm disp} \approx 2.3$ cm and $L_{\rm A} \approx 15.3$ cm, which can give a higher quantum-state fidelity for the qubit memory.

APPENDIX C: DERIVATION OF EQUATIONS (12a) AND (12b)

We start the derivation by applying the Laplace transformations

$$\bar{\hat{\mathcal{E}}}_j(p,\tau) \equiv \mathscr{L}_{z\to p}[\hat{\mathcal{E}}_j(z,\tau)] = \int_0^{+\infty} dz \hat{\mathcal{E}}_j(z,\tau) e^{-pz}, \quad \text{(C1a)}$$

$$\bar{\hat{\mathcal{S}}}_j(p,\tau) \equiv \mathscr{L}_{z\to p}[\hat{\mathcal{S}}_j(z,\tau)] = \int_0^{+\infty} dz \hat{\mathcal{S}}_j(z,\tau) e^{-pz}, \quad \text{(C1b)}$$

where the overbar' denotes the quantity in the Laplace domain and $\mathscr{L}_{z\to p}$ denotes the operation of the Laplace transformation with the argument changed from z to p. Substituting Eqs. (C1a) and (C1b) into Eqs. (11a) and (11b), and eliminating $\bar{\hat{\mathcal{E}}}_j$ with some algebras, we arrive at a first-order linear inhomogeneous differential equation for $\bar{\hat{\mathcal{S}}}_j$:

$$\left(i\frac{\partial}{\partial\tau} + d_{Sj} - \frac{|\Omega_c(\tau)|^2}{d_{Pj}}\frac{p}{p'_j}\right)\bar{\hat{\mathcal{S}}}_j - \frac{\Omega_c^*(\tau)}{d_{Pj}}\frac{1}{p'_j}\frac{G_p}{\sqrt{2}}\hat{\mathcal{E}}_j(0,\tau) = 0, \quad \text{(C2)}$$

where $p'_j = p + \delta_{Pj}\kappa_4\rho_{jj}^{(0)}$, $\delta_{Pj} = i\gamma_P/d_{Pj}$, and $\kappa_4 = |G_p|^2/(c\gamma_P)$. By performing the integration of the above equation over τ from $\tau = \tau_0$ and keeping in mind that $\Omega_c(\tau)$ are explicitly time dependent, we obtain

$$\begin{aligned}\bar{\hat{\mathcal{S}}}_j(p,\tau) = \bar{\hat{\mathcal{S}}}_j(p,\tau_0)\exp\left[id_{Sj}(\tau-\tau_0) - \frac{p}{p'_j}\kappa_c(\tau,\tau_0)\right] \\ - \frac{\delta_{Pj}}{\gamma_P}\int_{\tau_0}^{\tau} d\tau' \Omega_c^*(\tau')\frac{G_p}{\sqrt{2}}\hat{\mathcal{E}}_j(0,\tau')\frac{1}{p'_j} \\ \times \exp\left[id_{Sj}(\tau-\tau') - \frac{p}{p'_j}\kappa_c(\tau,\tau')\right], \quad \text{(C3)}\end{aligned}$$

where $\kappa_c(\tau_1,\tau_2) \equiv (\delta_{Pj}/\gamma_P)\int_{\tau_2}^{\tau_1} d\tau |\Omega_c(\tau)|^2$. By substituting Eq. (C3) into the Laplace form of Eqs. (11a) and (11b), one obtains the solutions of the operators of the signal field, given by

$$\begin{aligned}\bar{\hat{\mathcal{E}}}_j(p,\tau) = \frac{1}{p'_j}\hat{\mathcal{E}}_j(0,\tau) - \frac{\delta_{Pj}\kappa_4\sqrt{\rho_{jj}^{(0)}}}{G_p}\Omega_c(\tau)\bar{\hat{\mathcal{S}}}_j(p,\tau_0)\frac{1}{p'_j} \\ \times \exp\left[id_{Sj}(\tau-\tau_0) - \frac{p}{p'_j}\kappa_c(\tau,\tau_0)\right] \\ + \frac{\delta_{Pj}^2}{2\gamma_P}\kappa_4\Omega_c(\tau)\int_{\tau_0}^{\tau} d\tau' \Omega_c^*(\tau')\hat{\mathcal{E}}_j(0,\tau')\frac{1}{p'^2_j} \\ \times \exp\left[id_{Sj}(\tau-\tau') - \frac{p}{p'_j}\kappa_c(\tau,\tau')\right]. \quad \text{(C4)}\end{aligned}$$

Finally, by performing the inverse Laplace transformation on Eq. (C4), and noting that $\hat{\mathcal{S}}_j(z,\tau_0)$ can be neglected by assuming that there is no initial atomic coherence between the lower atomic states, we obtain Eqs. (12a) and (12b) given in the main text.

[1] A. I. Lvovsky, B. C. Sanders, and W. Tittel, Optical quantum memory, Nat. Photonics **3**, 706 (2009).

[2] K. Hammerer, A. S. Sørensen, and E. S. Polzik, Quantum interface between light and atomic ensembles, Rev. Mod. Phys. **82**, 1041 (2010).

[3] N. Sangouard, C. Simon, H. de Riedmatten, and N. Gisin, Quantum repeaters based on atomic ensembles and linear optics, Rev. Mod. Phys. **83**, 33 (2011).

[4] F. Bussières, N. Sangouarda, M. Afzeliusa, H. de Riedmattenb, C. Simon, and W. Tittel, Prospective applications of optical quantum memories, J. Mod. Opt. **60**, 1519 (2013).

[5] M. Afzelius, N. Gisin, and H. de Riedmatten, Quantum memory for photons, Phys. Today **68**(12), 42 (2015).

[6] K. Heshami, D. G. England, P. C. Humphreys, P. J. Bustard, V. M. Acosta, J. Nunn, and B. J. Sussman, Quantum memories: emerging applications and recent advances, J. Mod. Opt. **63**, 2005 (2016).

[7] D. Awschalom, K. K. Berggren, H. Bernien, S. Bhave, L. D. Carr, P. Davids, S. E. Economou, D. Englund, A. Faraon, M. Fejer, S. Guha, M. V. Gustafsson, E. Hu, L. Jiang, J. Kim, B. Korzh, P. Kumar, P. G. Kwiat, M. Lončar, M. D. Lukin *et al.*, Development of quantum interconnects (QuICs) for next-generation information technologies, PRX Quantum **2**, 017002 (2021).

[8] M. Fleischhauer, A. Imamoglu, and J. P. Marangos, Electromagnetically induced transparency: Optics in coherent media, Rev. Mod. Phys. **77**, 633 (2005).

[9] M. Fleischhauer and M. D. Lukin, Dark-State-Polaritons in Electromagnetically Induced Transparency, Phys. Rev. Lett. **84**, 5094 (2000).

[10] C. Liu, Z. Dutton, C. H. Behroozi, and L. V. Hau, Observation of coherent optical information storage in an atomic medium using halted light pulses, Nature (London) **409**, 490 (2001).

[11] D. F. Phillips, A. Fleischhauer, A. Mair, R. L. Walsworth, and M. D. Lukin, Storage of Light in Atomic Vapor, Phys. Rev. Lett. **86**, 783 (2001).

[12] I. Novikova, A. V. Gorshkov, D. F. Phillips, A. S. Sørensen, M. D. Lukin, and R. L. Walsworth, Optimal Control of Light

Pulse Storage and Retrieval, Phys. Rev. Lett. **98**, 243602 (2007).
[13] I. Novikova, N. B. Phillips, and A. V. Gorshkov, Optimal light storage with full pulse-shape control, Phys. Rev. A **78**, 021802(R) (2008).
[14] U. Schnorrberger, J. D. Thompson, S. Trotzky, R. Pugatch, N. Davidson, S. Kuhr, and I. Bloch, Electromagnetically Induced Transparency and Light Storage in an Atomic Mott Insulator, Phys. Rev. Lett. **103**, 033003 (2009).
[15] I. Novikova, R. L. Walsworth, and Y. Xiao, Electromagnetically induced transparency-based slow and stored light in warm atoms, Laser Photonics Rev. **6**, 333 (2012).
[16] Y.-H. Chen, M.-J. Lee, I.-C. Wang, S. Du, Y.-F. Chen, Y.-C. Chen, and I. A. Yu, Coherent Optical Memory with High Storage Efficiency and Large Fractional Delay, Phys. Rev. Lett. **110**, 083601 (2013).
[17] Y. O. Dudin, L. Li, and A. Kuzmich, Light storage on the time scale of a minute, Phys. Rev. A **87**, 031801(R) (2013).
[18] G. Heinze, C. Hubrich, and T. Halfmann, Stopped Light and Image Storage by Electromagnetically Induced Transparency Up to the Regime of One Minute, Phys. Rev. Lett. **111**, 033601 (2013).
[19] Y. Chen, Z. Bai, and G. Huang, Ultraslow optical solitons and their storage and retrieval in an ultracold ladder-type atomic system, Phys. Rev. A **89**, 023835 (2014).
[20] N. Šibalić, J. M. Kondo, C. S. Adams, and K. J. Weatherill, Dressed-state electromagnetically induced transparency for light storage in uniform-phase spin waves, Phys. Rev. A **94**, 033840 (2016).
[21] L. Ma, O. Slattery, and X. Tang, Optical quantum memory based on electromagnetically induced transparency, J. Opt. (Bristol) **19**, 043001 (2017).
[22] Y.-F. Hsiao, P.-J. Tsai, H.-S. Chen, S.-X. Lin, C.-C. Hung, C.-H. Lee, Y.-H. Chen, Y.-F. Chen, I.-A. Yu, and Y.-C. Chen, Highly Efficient Coherent Optical Memory Based on Electromagnetically Induced Transparency, Phys. Rev. Lett. **120**, 183602 (2018).
[23] Z. Bai, W. Li, and G. Huang, Stable single light bullets and vortices and their active control in cold Rydberg gases, Optica **6**, 309 (2019).
[24] A. Dantan, A. Bramati, and M. Pinard, Atomic quantum memory: Cavity versus single-pass schemes, Phys. Rev. A **71**, 043801 (2005).
[25] P. Barberis-Blostein and M. Bienert, Opacity of Electromagnetically Induced Transparency for Quantum Fluctuations, Phys. Rev. Lett. **98**, 033602 (2007).
[26] G. Hétet, A. Peng, M. T. Johnsson, J. J. Hope, and P. K. Lam, Characterization of electromagnetically-induced-transparency based continuous-variable quantum memories, Phys. Rev. A **77**, 012323 (2008).
[27] J. Appel, E. Figueroa, D. Korystov, M. Lobino, and A. I. Lvovsky, Quantum Memory for Squeezed Light, Phys. Rev. Lett. **100**, 093602 (2008).
[28] K. Honda, D. Akamatsu, M. Arikawa, Y. Yokoi, K. Akiba, S. Nagatsuka, T. Tanimura, A. Furusawa, and M. Kozuma, Storage and Retrieval of a Squeezed Vacuum, Phys. Rev. Lett. **100**, 093601 (2008).
[29] D.-S. Ding, Z.-Y. Zhou, B.-S. Shi, and G.-C. Guo, Single-photon-level quantum image memory based on cold atomic ensembles, Nat. Commun. **4**, 2527 (2013).
[30] Y.-L. Chuang, I. A. Yu, and R.-K. Lee, Quantum theory for pulse propagation in electromagnetically-induced-transparency media beyond the adiabatic approximation, Phys. Rev. A **91**, 063818 (2015).
[31] L. Li and A. Kuzmich, Quantum memory with strong and controllable Rydberg-level interactions, Nat. Commun. **7**, 13618 (2016).
[32] S. J. Yang, J. Rui, H. N. Dai, X. M. Jin, S. Chen, and J.-W. Pan, High-contrast transparency comb of the electromagnetically-induced-transparency memory, Phys. Rev. A **98**, 033802 (2018).
[33] X.-D. Tian, Y.-M. Liu, Q.-Q. Bao, J.-H. Wu, M. Artoni, and G. C. La Rocca, Nonclassical storage and retrieval of a multiphoton pulse in cold Rydberg atoms, Phys. Rev. A **97**, 043811 (2018).
[34] L. Yang, B. He, and M. Xiao, Storage and retrieval of interacting photons in a Rydberg medium, Phys. Rev. A **99**, 043827 (2019).
[35] P. Kok, W. J. Munro, K. Nemoto, T. C. Ralph, J. P. Dowling, and G. J. Milburn, Linear optical quantum computing with photonic qubits, Rev. Mod. Phys. **79**, 135 (2007).
[36] T. Chanelière, D. N. Matsukevich, S. D. Jenkins, S.-Y. Lan, T. A. B. Kennedy, and A. Kuzmich, Storage and retrieval of single photons transmitted between remote quantum memories, Nature (London) **438**, 833 (2005).
[37] K. S. Choi, H. Deng, J. Laurat, and H. J. Kimble, Mapping photonic entanglement into and out of a quantum memory, Nature (London) **452**, 67 (2008).
[38] Y.-W. Cho and Y.-H. Kim, Atomic vapor quantum memory for a photonic polarization qubit, Opt. Express **18**, 25786 (2010).
[39] H. Zhang, X.-M. Jin, J. Yang, H.-N. Dai, S.-J. Yang, T.-M. Zhao, J. Rui, Y. He, X. Jiang, F. Yang, G.-S. Pan, Z.-S. Yuan, Y. Deng, Z.-B. Chen, X.-H. Bao, S. Chen, B. Zhao, and J.-W. Pan, Preparation and storage of frequency-uncorrelated entangled photons from cavity-enhanced spontaneous parametric down-conversion, Nat. Photonics **5**, 628 (2011).
[40] M. Lettner, M. Mücke, S. Riedl, C. Vo, C. Hahn, S. Baur, J. Bochmann, S. Ritter, S. Dürr, and G. Rempe, Remote Entanglement between a Single Atom and a Bose-Einstein Condensate, Phys. Rev. Lett. **106**, 210503 (2011).
[41] S. Zhou, S. Zhang, C. Liu, J. F. Chen, J. Wen, M. M. T. Loy, G. K. L. Wong, and S. Du, Optimal storage and retrieval of single-photon waveforms, Opt. Express **20**, 24124 (2012).
[42] S. Riedl, M. Lettner, C. Vo, S. Baur, G. Rempe, and S. Durr, Bose-Einstein condensate as a quantum memory for a photonic polarization qubit, Phys. Rev. A **85**, 022318 (2012).
[43] Z. Xu, Y. Wu, L. Tian, L. Chen, Z. Zhang, Z. Yan, S. Li, H. Wang, C. Xie, and K. Peng, Long Lifetime and High-Fidelity Quantum Memory of Photonic Polarization Qubit by Lifting Zeeman Degeneracy, Phys. Rev. Lett. **111**, 240503 (2013).
[44] N. Kalb, A. Reiserer, S. Ritter, and G. Rempe, Heralded Storage of a Photonic Quantum Bit in a Single Atom, Phys. Rev. Lett. **114**, 220501 (2015).
[45] V. Parigi, V. D'Ambrosio, C. Arnold, L. Marrucci, F. Sciarrino, and J. Laurat, Storage and retrieval of vector beams of light in a multiple-degree-of-freedom quantum memory, Nat. Commun. **6**, 7706 (2015).
[46] C. Kupchak, T. Mittiga, B. Jordaan, M. Namazi, C. Nölleke, and E. Figueroa, Room-temperature single-photon level memory for polarization states, Sci. Rep. **5**, 7658 (2015).

[47] L. Chen, Z. Xu, W. Zeng, Y. Wen, S. Li, and H. Wang, Controllably releasing long-lived quantum memory for photonic polarization qubit into multiple spatially-separate photonic channels, Sci. Rep. **6**, 33959 (2016).

[48] M. Namazi, G. Vallone, B. Jordaan, C. Goham, R. Shahrokhshahi, P. Villoresi, and E. Figueroa, Free-Space Quantum Communication with a Portable Quantum Memory, Phys. Rev. Appl. **8**, 064013 (2017).

[49] M. Körber, O. Morin, S. Langenfeld, A. Neuzner, S. Ritter, and G. Rempe, Decoherence-protected memory for a single-photon qubit, Nat. Photonics **12**, 18 (2018).

[50] P. Vernaz-Gris, K. Huang, M. Cao, A. S. Sheremet, and J. Laurat, Highly-efficient quantum memory for polarization qubits in a spatially-multiplexed cold atomic ensemble, Nat. Commun. **9**, 363 (2018).

[51] Y. Wang, J. Li, S. Zhang, K. Su, Y. Zhou, K. Liao, S. Du, H. Yan, and S.-L. Zhu, Efficient quantum memory for single-photon polarization qubits, Nat. Photonics **13**, 346 (2019).

[52] A. V. Gorshkov, A. A. André, M. Fleischhauer, A. S. Sørensen, and M. D. Lukin, Universal Approach to Optimal Photon Storage in Atomic Media, Phys. Rev. Lett. **98**, 123601 (2007).

[53] A. V. Gorshkov, A. André, M. D. Lukin, and A. S. Sørensen, Photon storage in Λ-type optically dense atomic media. I. Cavity model, Phys. Rev. A **76**, 033804 (2007).

[54] A. V. Gorshkov, A. André, M. D. Lukin, and A. S. Sørensen, Photon storage in Λ-type optically dense atomic media. II. Free-space model, Phys. Rev. A **76**, 033805 (2007).

[55] R. Zhang and X.-B. Wang, Storage efficiency of probe pulses in an electromagnetically-induced-transparency medium, Phys. Rev. A **94**, 063856 (2016).

[56] A. Grodecka-Grad, E. Zeuthen, and A. S. Sørensen, High-Capacity Spatial Multimode Quantum Memories Based on Atomic Ensembles, Phys. Rev. Lett. **109**, 133601 (2012).

[57] E. Zeuthen, A. Grodecka-Grad, and A. S. Sørensen, Three-dimensional theory of quantum memories based on Λ-type atomic ensembles, Phys. Rev. A **84**, 043838 (2011).

[58] U. Leonhardt, *Measuring the Quantum State of Light* (Cambridge University Press, New York, 1997).

[59] A. I. Lvovsky and M. G. Raymer, Continuous-variable optical quantum state tomography, Rev. Mod. Phys. **81**, 299 (2009).

[60] D. Petrosyan and Y. P. Malakyan, Magneto-optical rotation and cross-phase modulation via coherently driven four-level atoms in a tripod configuration, Phys. Rev. A **70**, 023822 (2004).

[61] The wave numbers in the definition of $\hat{S}_{\beta\alpha}$ are given by $k_1 = k_2 \equiv 0$, $k_3 = k_p - k_c$, $k_4 = k_p$. In the Schrödinger picture, $\hat{\sigma}^j_{\alpha\beta} \equiv |\alpha\rangle_{jj}\langle\beta|$, with $|\alpha\rangle_j$ being the energy eigenstate $|\alpha\rangle$ of the jth atom.

[62] S. M. Barnett and P. M. Radmore, *Methods in Theoretical Quantum Optics* (Clarendon, Oxford, 1997).

[63] L. Mandel and E. Wolf, *Optical Coherence and Quantum Optics* (Cambridge University Press, New York, 1995).

[64] D. A. Steck, Rubidium 87 D line data, https://steck.us/alkalidata/.

[65] N. B. Phillips, A. V. Gorshkov, and I. Novikova, Slow light propagation and amplification via electromagnetically induced transparency and four-wave mixing in an optically dense atomic vapor, Phys. Rev. A **83**, 063823 (2011).

[66] N. Lauk, C. O'Brien, and M. Fleischhauer, Fidelity of photon propagation in electromagnetically induced transparency in the presence of four-wave mixing, Phys. Rev. A **88**, 013823 (2013).

[67] J. Wu, Y. Liu, D.-S. Ding, Z.-Y. Zhou, B.-S. Shi, and G.-C. Guo, Light storage based on four-wave mixing and electromagnetically induced transparency in cold atoms, Phys. Rev. A **87**, 013845 (2013).

[68] J. Geng, G. T. Campbell, J. Bernu, D. B. Higginbottom, B. M. Sparkes, S. M. Assad, W. P. Zhang, N. P. Robins, P. K. Lam, and B. C. Buchler, Electromagnetically induced transparency and four-wave mixing in a cold atomic ensemble with large optical depth, New J. Phys. **16**, 113053 (2014).

[69] Q. Zhang and G. Huang, Suppression of quantum noise by two-mode squeezed states for photon propagation under conditions of electromagnetically induced transparency and four-wave mixing, Phys. Rev. A **101**, 033806 (2020).

[70] These bosonic operators obey the standard equal-t bosonic commutation relations $[\hat{\mathcal{E}}_j(z,t), \hat{\mathcal{E}}^\dagger_{j'}(z',t)] = [\hat{\mathcal{P}}_j(z,t), \hat{\mathcal{P}}^\dagger_{j'}(z',t)] = [\hat{\mathcal{S}}_j(z,t), \hat{\mathcal{S}}^\dagger_{j'}(z',t)] = \delta(z-z')\delta_{jj'}$.

[71] The form of the time-dependent control field assumed here is just a simple mathematical description for its switching on and off for realizing the qubit QM, used in the numerical simulation given in Sec. III B. In principle, it can be switching functions with different forms, and hence the analytical approach given in this section is valid for different control fields.

[72] R. Loudon, *The Quantum Theory of Light*, 3rd ed. (Oxford University Press, New York, 2000).

[73] The maximum memory efficiency is found to be $\eta_{\max} \approx 0.71$, obtained at the optical depth $D \approx 112$. This optical depth is very close to the optimal optical depth $D^{\text{opt}} = 110$ for acquiring the maximum quantum-state fidelity.

[74] Due to the symmetry of the system, the wave form of the σ^- component is basically the same as that of the σ^+ component. To show them clearly in the figure, the wave form of the σ^- component has been multiplied by 0.8 (dashed blue line 2).

[75] D. Schraft, M. Hain, N. Lorenz, and T. Halfmann, Stopped Light at High Storage Efficiency in a Pr^{3+}:Y_2SiO_5 Crystal, Phys. Rev. Lett. **116**, 073602 (2016).

[76] P. Kok and B. W. Lovett, *Introduction to Optical Quantum Information Processing* (Cambridge University Press, New York, 2010).

[77] The wave forms of $|\Phi_{Ej}|/|\Phi_{E0}|_{\max}$ $(j = 1, 2, 3)$ nearly coincide with each other. To make the difference in the figure, the wave forms of $|\Phi_{E1}|/|\Phi_{E0}|_{\max}$ and $|\Phi_{E2}|/|\Phi_{E0}|_{\max}$ are multiplied by 1.5 (solid red line) and by 1.3 (dashed blue line), respectively.

[78] Y. H. Shih, *An Introduction to Quantum Optics: Photon and Biphoton Physics* (CRC, Boca Raton, 2011).